Journal of Inflammation Research

Dovepress
Taylor & Francis Group

Open Access Full Text Article

ORIGINAL RESEARCH

Protective Effects of Qingre Sanjie Jiaonang on Pulmonary Fibrosis: A Pilot Study

Liu-Cheng Li[1,*], Zhi-Hui Zhang[2,*], Lei Liu[3,*], Bo Chen[1,*], Ye-Cheng Jin[1], Yu-Zhen Wang[1]

[1]Department of Pharmacy, Sir Run Run Shaw Hospital, Zhejiang University School of Medicine, Hangzhou, 310016, People's Republic of China; [2]Shanghai TCM-Integrated Hospital, Shanghai University of Traditional Chinese Medicine, Shanghai, 200082, People's Republic of China; [3]Department of Orthopaedics, Shaoxing Hospital of Traditional Chinese Medicine, Shaoxing, 312000, People's Republic of China

*These authors contributed equally to this work

Correspondence: Yu-Zhen Wang; Ye-Cheng Jin, Sir Run Run Shaw Hospital, Zhejiang University School of Medicine, No. 3 Qingchun East Road, Hangzhou, 310016, People's Republic of China, Email 3299024@zju.edu.cn; jinyecheng_lab@163.com

Background: Qingre Sanjie Jiaonang (QRSJ) is a single herbal preparation from Senecio scandens Buch.-Ham.ex D. Don which has been proved to have anti-inflammatory and antioxidant effects. QRSJ has been used in treating upper respiratory tract inflammation and acute bronchitis in China for nearly twenty years.

Purpose: This study aims to explore the potential effects of QRSJ in alleviating pulmonary fibrosis (PF) and its mechanisms.

Study Design and Method: A mouse model of PF was induced by intratracheal injection of Bleomycin (BLM, 5 mg/kg), followed by different doses of QRSJ administration (0.5 g/kg, 1.0 g/kg) for 28 days. The lung tissues were collected and prepared for Hematoxylin-Eosin (H&E) staining to observe the pathological changes, while Masson staining was for determining collagen production. RNA sequencing (RNA-seq), flow cytometry and immunofluorescence experiments were employed to investigate the impact of QRSJ on the immune microenvironment. The expression levels of IL-1β, IL-6, CXCL15 (mouse homologue of human IL-8), and TNF-α in the bronchoalveolar lavage fluid (BALF) and serum of mice were observed. Besides, the levels of high mobility group protein B1 (HMGB1), an inflammatory and profibrotic mediator, in the BALF, serum and lung tissues of mice were also detected.

Results: The mouse model of PF was successfully established by checking the pathological examinations. With QRSJ intervention, BLM-induced destruction of alveolar structure and inflammatory cell infiltration were alleviated. H&E results further revealed that the administration of BLM and QRSJ had no impact on kidney histological structure of mice. Meanwhile, QRSJ inhibited the deposition of collagen, decreased the expression of fibronectin and lumican. Next, QRSJ treatment improved immune cell infiltration in the lung, along with the down-regulation of CD45 and Ly6G, and led to a decrease in the immune cell count in BALF. Furthermore, QRSJ alleviated the release of inflammatory factors, including NE, IL-1β, IL-6, CXCL15, and TNF-α. Besides, QRSJ significantly reduced the level of proinflammatory cytokine HMGB1.

Conclusion: This study demonstrated the benefits of QRSJ in improving the pathological abnormalities in a PF model, revealing the new potential of the old drug. It should be attributed to the regulation of abnormal immune microenvironment and HMGB1 release. Future efforts should focus on its specific pharmacological mechanisms and clinical outcomes.

Keywords: Qingre Sanjie Jiaonang, pulmonary fibrosis, HMGB1

Introduction

Pulmonary fibrosis (PF) is characterized by excessive deposition of extracellular matrix (ECM), superabundant proliferation of myofibroblasts, and exorbitant remodeling of lung tissue structure.[1–3] Several decades of research have contributed to a better understanding of its pathogenesis, though only two drugs, Nintedanib and Pirfenidone, thus far have shown treatment efficacy by slowing the decline of lung function.[4,5] Emerging efforts continue to explore new agents for treating PF, most notably the use of old drugs.

Traditional Chinese medicine is a medical treasure that Chinese people have used for thousands of years, and it has played an important role in preventing and treating serious lung diseases.[6–8] Qingre Sanjie Jiaonang (QRSJ) is a single

Received: 27 July 2024
Accepted: 21 March 2025
Published: 31 March 2025

Graphical Abstract

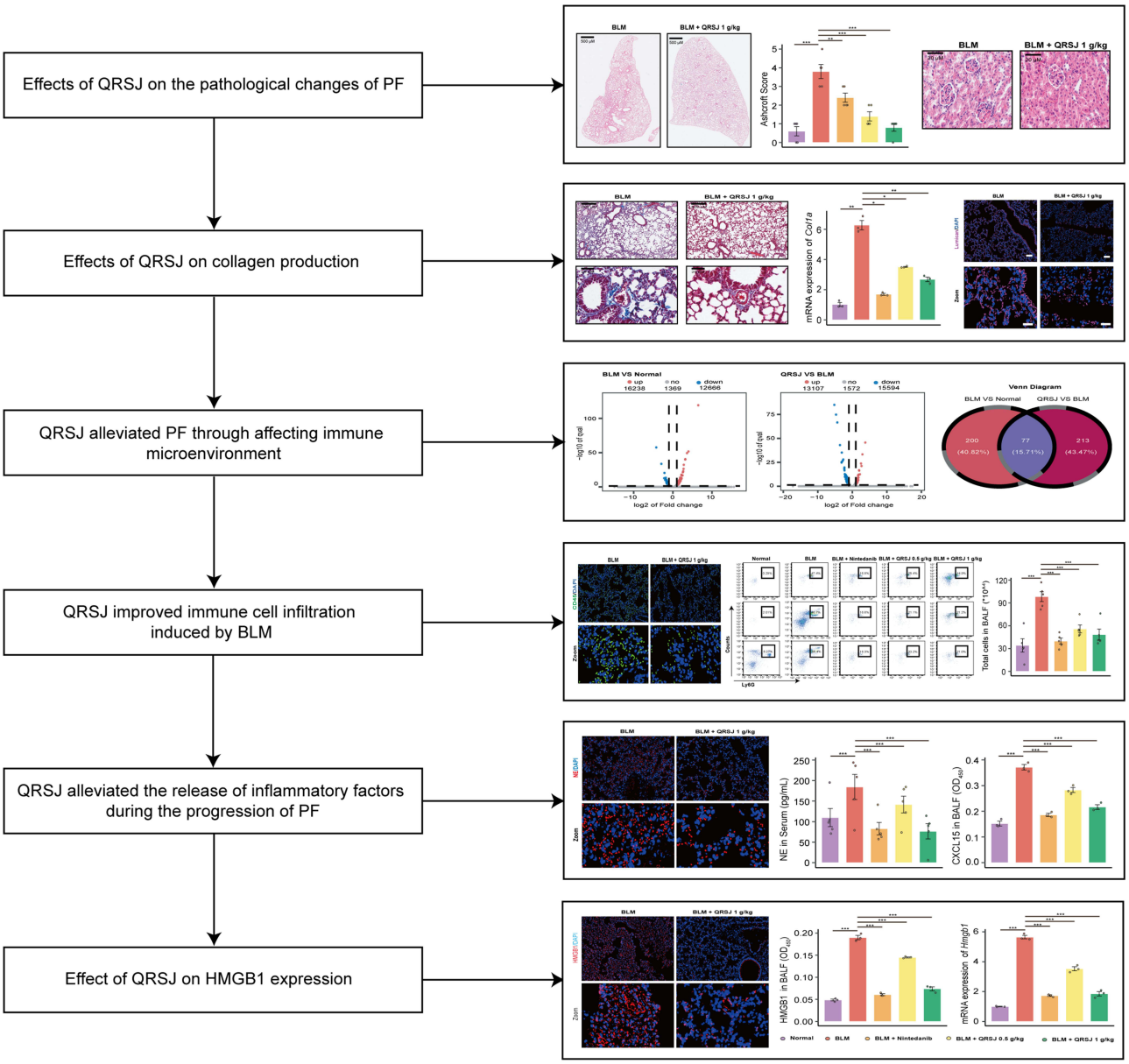

herbal preparation extracted from *Senecio scandens* Buch.-Ham.ex D. Don, which contains a large number of valuable compounds, including flavonoids, alkaloids, phenolic acids, terpenes, and polysaccharides.[9,10] QRSJ has been clinically used in the treatment of upper respiratory tract inflammation and acute bronchitis in China for nearly two decades. Its herbal composition, *Senecio scandens* Buch.-Ham.ex D. Don, has been proved to have anti-inflammatory and antioxidant effects.[10]

Chronic inflammation is the key feature of PF and is driven by both innate and adaptive immune responses.[11–13] During the PF development, various immune cells and activated fibroblasts secrete various pro-inflammatory cytokines and chemokines, thereby perpetuating the inflammatory response and contributing to the recruitment and activation of more immune cells and fibroblasts.[14,15] The balance between pro-inflammatory and regulatory immune cell subsets, as

well as the interactions between immune cell types and resident cells within the lung microenvironment, ultimately determines the extent of fibrosis and the potential for resolution.[14,16,17]

High mobility group protein B1 (HMGB1) is a recognized mediator and culprit of cascade inflammatory damage and fibrosis.[18–20] It is a nonhistone nuclear protein that has multiple functions according to its subcellular location. After its active secretion or passive release, extracellular HMGB1 usually acts as a damage-associated molecular pattern (DAMP) molecule, regulating inflammation and immune responses through different receptors or direct uptake.[21,22] In recent years, we found that HMGB1 was a potential therapeutic target for PF, down-regulated expression of which was associated with inhibited proliferation of profibrotic myofibroblasts and reduced protein levels of ECM.[23–26] Other researchers have also confirmed the key role of HMGB1 in renal fibrosis, liver fibrosis, and myocardial fibrosis.[27–29] These results all support that HMGB1 is a key regulator in fibrotic diseases. However, it is unclear whether QRSJ can affect the process of lung injury and PF, and the role of HMGB1 during QRSJ treatment is also a mystery to be discovered. To explore the effects of QRSJ in PF, we conducted the first study to investigate its role in pathologic changes of lungs and HMGB1 level in a PF mouse model.

Materials and Methods

Materials

Bleomycin was purchased from Laiboten Pharmaceutical (Haerbin, China). Enzyme-linked immunosorbent assay (ELISA) Kits for tumor necrosis factor (TNF)-α (Cat # E-EL-M3063), IL-6 (Cat # E-EL-M0044), CXCL15 (mouse homologue of human IL-8, Cat # E-EL-M0269), HMGB1 (Cat # E-EL-M0676), IL-1β (Cat # E-EL-M0037) and NE (Cat # E-EL-M3025) were purchased from Elabscience (Wuhan, China). Qingre Sanjie Jiaonang was purchased from Hunan Tianji Caotang Pharmaceutical Co. Anti-CD45 (Cat # ab40763), and anti-Neutrophil elastase (NE, Cat # ab131260) were purchased from Abcam (Cambridge, USA). Anti-HMGB1 (Cat # bs-0664R) was purchased from Bioss Biotechnology (Beijing, China). Anti-Ly6G (Cat # 65078) and anti-Lumican (Cat # 10677-1-AP) were purchased from Proteintech (Wuhan, China). Alexa Fluor 488 Goat anti-mouse IgG (H+L) Secondary Antibody (Cat # A11001) and Alexa Fluor 594 Goat anti-Rabbit IgG (H+L) Secondary Antibody (Cat # A11037) were purchased from ThermoFisher Scientific (Waltham, MA). Hematoxylin-Eosin (H&E) stain kit (Cat # G1120) and Masson's trichrome stain kit (Cat # G1340) were purchased from Solarbio Science & Technology Co., Ltd (Beijing, China).

Establishment of PF Model

Eight-week-old male C57BL/6 mice were placed in a pathogen-free environment, and adaptively fed for one week before the in vivo experiments. The mice were randomly divided into five groups: normal group, Bleomycin (BLM, 5 mg/kg) group, QRSJ 0.5 g/kg group, QRSJ 1 g/kg group, and Nintedanib (50 mg/kg) group, with 5 mice in each group. BLM group, QRSJ 0.5 g/kg group, QRSJ 1 g/kg group and Nintedanib group were injected with BLM into the trachea at one time to reproduce the PF model. BLM was dissolved in 0.9% sodium chloride injection with a volume of 1.6 mL just before use. The normal group was given 0.9% sodium chloride instead. All mice injected with BLM or saline were rotated upright immediately after BLM injection so that the liquid could be evenly distributed in the whole lungs. Since the next day of modeling, mice in QRSJ 0.5 g/kg group, QRSJ 1 g/kg group, and Nintedanib group were given 0.5 g/kg, 1 g/kg QRSJ and 50 mg/kg Nintedanib by intragastric administration, respectively. The mouse dose of QRSJ 0.5 g/kg group is translated from the recommended daily dose for adults according to "equivalent dose ratio table of human and animal body surface area". The animal experimental protocol was in accordance with the Guidelines for the Care and Use of Experimental Animals issued by the National Institute of Health, and approved by Zhejiang University Laboratory Animal Welfare and Ethics Review Committee (No. ZJU20240288).

All intragastric drugs were prepared in suspension of experimental concentration in 0.5% sodium carboxymethyl cellulose. Mice in normal group and BLM group were given 0.5% sodium carboxymethyl cellulose in the same way

every day. On the 28th day after modeling, the lung tissues, bronchoalveolar lavage fluid (BALF), serum and kidney tissues of the mice were collected, while other tissues were not.

H&E Staining

The left lobes of lung tissues and kidney tissues of the mice were collected and fixed in 10% formaldehyde solution for two days, then dehydrated, embedded in paraffin, and cut into 5 μm thick slices using a microtome, and stained with the H&E kit. The slices were dewaxed in xylene twice for 5–10 min each time. A series of ethanol (100%, 95%, 85%, 75%) was used to rehydrate the slices with 3 min per gradient. Then, the slices were soaked in distilled water for 2 min, stained nucleus with Hematoxylin Solution for 2–10 min and rinsed in running tap water. Subsequently, the slices were differentiated with Differentiation Solution for 10–60s, rinsed with tap water twice for 3–5 min each, and re - dyed with Eosin Solution for 10s to 2 min. Finally, the slices underwent dehydration, clearing and sealed with resin. The images were observed and collected under an optical microscope. The Ashcroft score[30] was applied to assess the fibrosis of the lungs.

Masson Staining

The paraffin-embedded lung tissues were cut into 5 um thick slices using a microtome, and stained with the Masson's trichrome stain kit. The slices were dewaxed to distilled water, stained with Weigert's Iron Hematoxylin Solution for 5–10 min, washed with distilled water to remove excess stain, differentiated with Acid Differentiation for 5–10s, and washed with distilled water for 30s again. Then, the slices were stained with Bluing Solution for 3–5 min, rinsed in distilled water for 30s, stained with Ponceau-Acid Fuchsin Solution for 5–10 min and rinsed with Weak Acid Working Solution for 30s. Subsequently, the slices were differentiated in Phosphomolybdic Acid Solution for 1–2 min and stained with Aniline Blue Solution for 1–2 min. Finally, the slices underwent dehydration, clearing and sealed with resin. The images were observed and collected under an optical microscope. The staining results were that collagen fibers were dyed blue, while muscle and elastic fibers were dyed red.

Enzyme-Linked Immunosorbent Assay (ELISA)

BALF and serum were extracted from the mice. All of the samples were centrifuged at 3000 rpm for 10 min, and then the liquid supernatant was collected to detect the level of TNF-α, IL-6, CXCL15, IL-1β, NE and HMGB1 by using ELISA kits according to the kit instruction.

Immunofluorescence Staining

Immunofluorescence staining for CD45 (1:100), Ly6G (1:100), NE (1:70), Lumican (1:200), and HMGB1 (1:100) was carried out. The slices were deparaffinized and rehydrated. Antigen retrieval was conducted in a pH 9.0 EDTA buffer, utilizing a water bath maintained at 100 °C for 20 min. The slices were incubated in 3% hydrogen peroxide solution at room temperature for 15 min away from light. Subsequently, slices were blocked with 3% goat serum for 30 min at room temperature, and then incubated with the primary antibody overnight at 4 °C. Sections were washed thrice with PBS and subsequently incubated with poly-HRP secondary antibody of the corresponding species at room temperature for 20 min away from light. Cell nuclei were stained with DAPI for 10 min. Finally, the tissue sections were sealed, and the images were observed and collected by fluorescence microscope.

BALF Analysis by Flow Cytometry

The lung tissues of mice were infused with ice-cold PBS and washed three times. The total number of BALF cells was detected, and the BALF cells were incubated with anti-mouse CD45-AF700 and Ly6G-PE/Cy7 in PBS. The number of immune cells was determined by Fluorescence-activated cell sorting (FACS) analysis.

Realtime-Quantitative Polymerase Chain Reaction (RT-qPCR)

The lung tissues were subjected to mRNA extraction using Trizol reagent. Subsequently, the extracted mRNA was reverse transcribed into cDNA and amplified using Hi Script ® II qRT Super Mix (Vazyme, China). Real-time fluorescent quantitative

PCR analysis was conducted on a Bio-Rad sequence detection system using Taq Pro Universal SYBR qPCR Master Mix (Vazyme, China). The Nanjing GenScript Company synthesized the primers (mouse Collagen-I (*Col1a*): forward 5′-GCTCCTCTTAGGGGCCACT-3′ and reverse 5′-ATTGGGGACCCTTAGGCCAT-3′; mouse *Hmgb1*: forward 5′-GCTGACAAGGCTCGTTATGAA-3′and reverse 5′-CCTTTGATTTTGGGGCGGTA-3′; mouse Fibronectin (*Fn1*): forward 5′-ATGTGGACCCCTCCTGATAGT-3′and reverse 5′-GCCCAGTGATTTCAGCAAAGG-3′; mouse *GAPDH*: forward 5′-AGGTCGGTGTGAACGGATTTG-3′and reverse 5′-GGGGTCGTTGATGGCAACA-3′) according to the GenBank serial number. PCR reaction conditions were strictly followed: 95 °C for 5 min initially, then 55 cycles. Each cycle included 95 °C for 10s and 60 °C for 30s. In order to compare the relative gene expression levels, the Ct value of the gene was calculated through the $2^{-\Delta\Delta Ct}$ method.

RNA Sequencing (RNA-Seq) Analysis

Total RNA was obtained from mouse lung tissue by employing Trizol, chloroform, and isopropanol, and subsequently quantified by Nanodrop (Thermo, USA) with 1 μL. The construction of an RNA library involves several steps: purifying and fragmenting mRNA, synthesizing the first strand of cDNA, synthesizing the second strand of cDNA, performing end repair, adenylating the 3' ends, ligating adapters, and enriching DNA fragments. NovaSeq 6000 (Illumina, USA) was used to sequence. The RNA-seq data has been uploaded to the NCBI website (www.ncbi.nlm.nih.gov), and the BioProject number is PRJNA1209374.

Statistical Analyses

All data were shown as the mean ± standard deviation (SD). Statistical analysis was performed by SPSS 26.0 software. The difference among multiple groups was performed by one-way analysis of variance (ANOVA), followed by using a post hoc LSD test or Games-Howell test. Column graphs were drawn using RStudio. Statistical significance was set at $*p < 0.05$, $**p < 0.01$, and $***p < 0.001$.

Results

Effects of QRSJ on the Pathological Changes of PF

In order to investigate the intervention effects of QRSJ on PF, we used QRSJ to intervene in BLM-induced mice (Figure 1A), and observed the effects of QRSJ on BLM-induced pathological changes in lung tissues. In the BLM induced mice, it was confirmed that the alveolar structure was obviously destroyed at 28 days after BLM modeling. Meanwhile, the inflammatory cells were infiltrated, and the alveolar intervals were significantly thickened. These pathological features suggest the success of PF model. After different doses of QRSJ intervention, BLM-induced abnormal changes were reversed (Figure 1B and C). In addition, we have collected mice kidney tissues of each group. H&E results revealed that the administration of BLM and QRSJ had no impact on kidney histological structure of mice (Figure 1D). It indicated that QRSJ improved the pathological changes of experimental PF without affecting the kidney.

Effects of QRSJ on Collagen Production

Collagen deposition is one of the main characteristics of fibrotic diseases.[31,32] In order to investigate the effect of QRSJ on collagen secretion (one of the main components of the ECM), Masson staining was used to observe its effects on BLM-induced mice. In the BLM-induced groups, different degrees of alveolar structure destruction and collagen expression (blue regions) were observed in mice. Compared with the BLM group, collagen expression in the QRSJ groups was significantly reduced, and the degree of PF was alleviated (Figure 2A and B). Besides, RT-qPCR was used to observe the mRNA expression of *Col1a* and *Fn1*. Immunofluorescence staining was employed to observe the expression of lumican, as another marker protein of ECM deposition. The results showed that after administration of QRSJ, the expression levels of *Col1a, Fn1*, and lumican were significantly decreased compared with the BLM group (Figure 2C–F). It indicated that QRSJ could inhibit the production of collagen and reduce the degree of fibrotic injury.

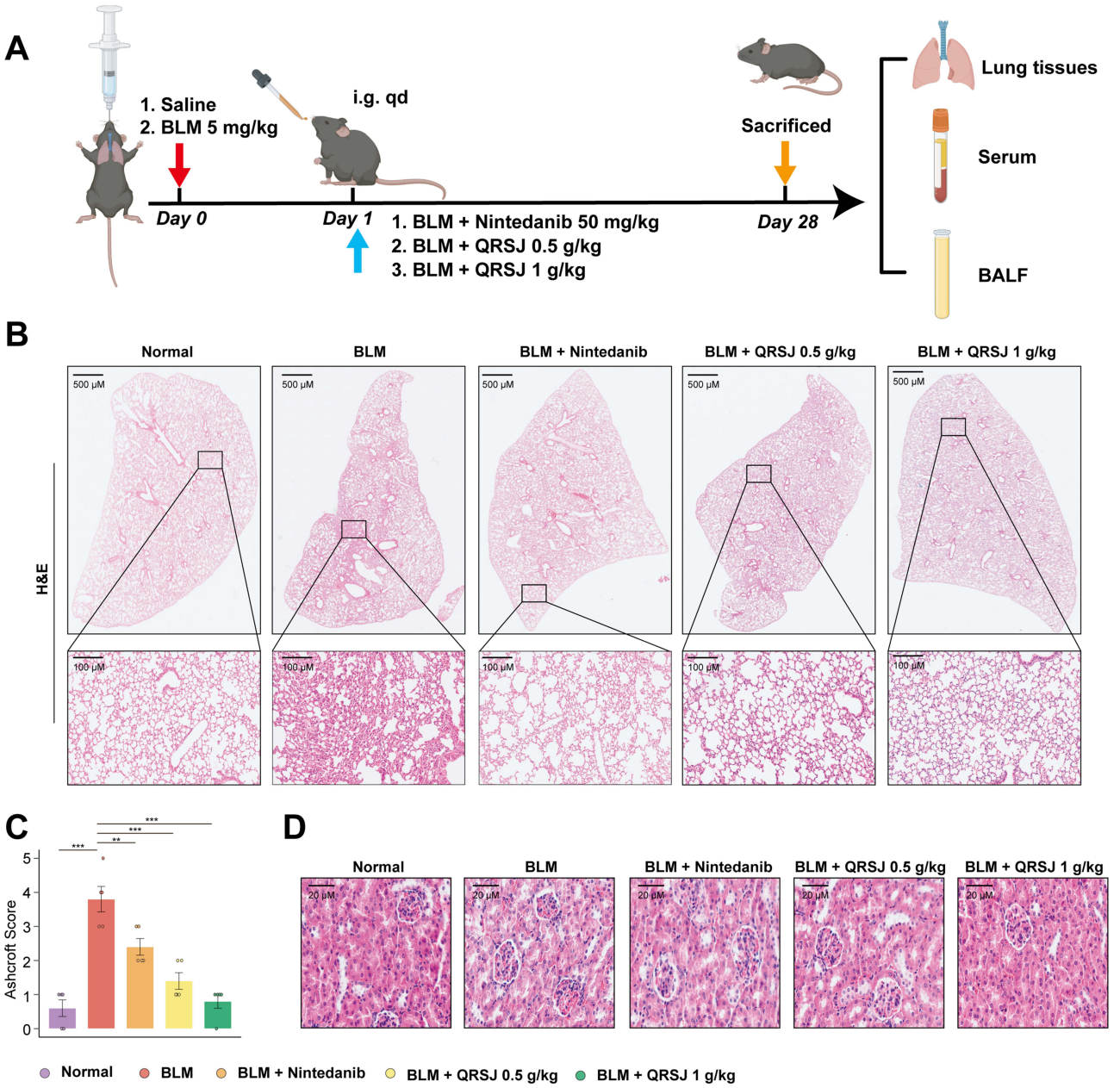

Figure 1 Effects of QRSJ on the pathological changes in mice with PF. (**A**) Schematic diagram of in vivo experimental modeling and grouping. (**B**) Image of H&E staining of the lung tissues (Scale bar, 500 μm or 100 μm). (**C**) The bar graph illustrates the Ashcroft score to evaluate the degree of PF observed in the H&E assay. (**D**) Image of H&E staining of the kidney tissues (Scale bar, 20 μm). The data is presented as mean ± SD (n = 5), $^{**}p < 0.01$ and $^{***}p < 0.001$ by one-way ANOVA.

QRSJ Alleviated PF Through Affecting Immune Microenvironment

RNA-seq is a recently developed approach to transcriptome profiling that uses deep-sequencing technologies.[33] In this study, RNA-seq was further performed on the lung tissues of mice in normal group, BLM group and BLM + 1 g/kg QRSJ group. Compared with normal group, there were a total of 30273 differential mRNAs, of which 16238 were up-regulated and 12666 were down-regulated in BLM group (Figure 3A). Compared with BLM group, there were a total of 30273 differential mRNAs, of which 13107 were up-regulated and 15594 were down-regulated in BLM+QRSJ group (Figure 3B). A total of 77 differential mRNAs were disturbed in BLM group and were reverted after the intervention of QRSJ, which were shown in the venn diagram and cluster analysis (Figure 3C). GSEA enrichment analysis was further performed on differential genes from BLM + QRSJ

 https://doi.org/10.2147/JIR.S479432

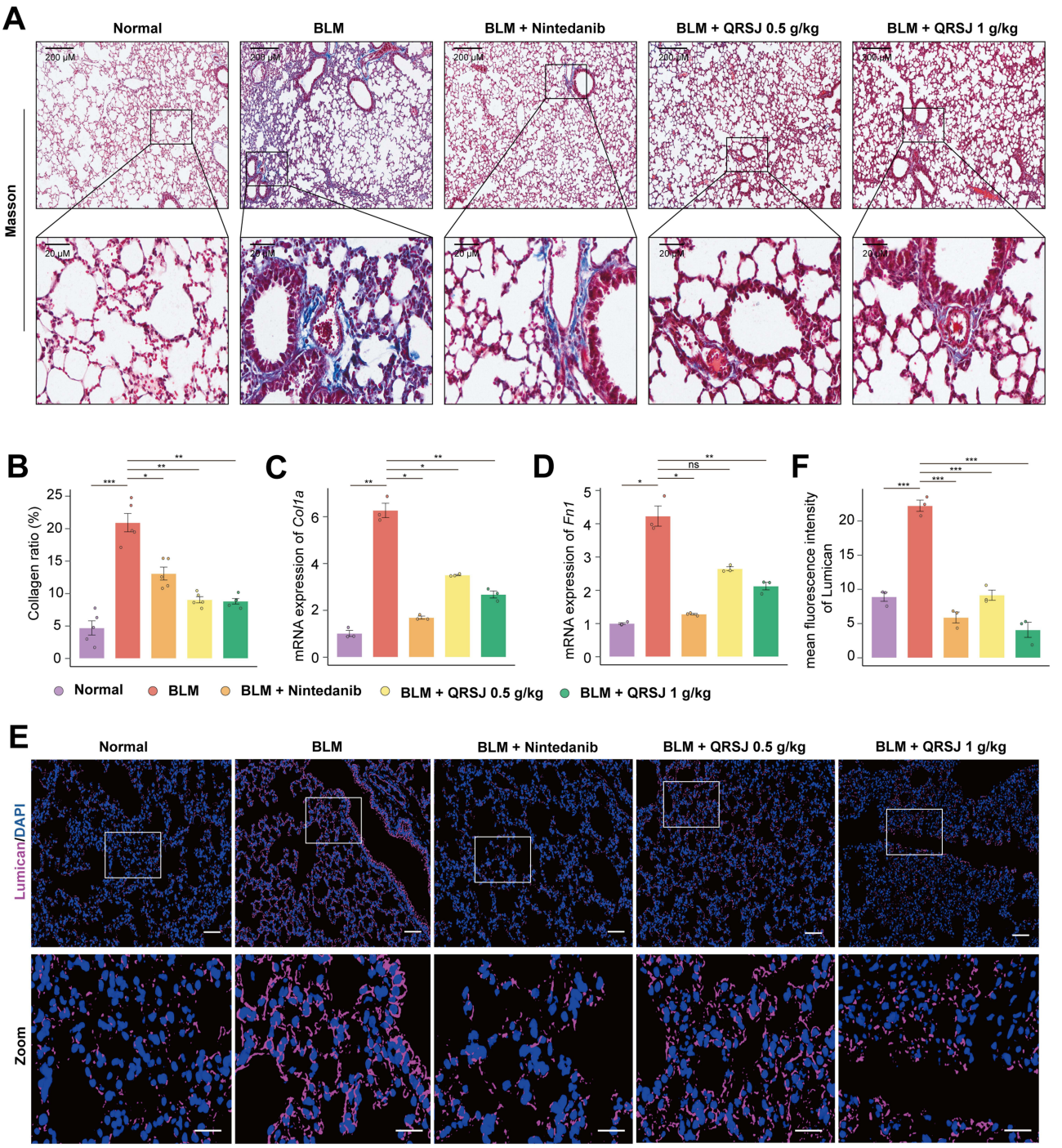

Figure 2 Effects of QRSJ on collagen production in mice with PF. (**A**) Image of Masson staining of the lung tissues (Scale bar, 200 μm or 20 μm). (**B**) The bar graph illustrates the area of collagen deposition according to Masson assay (n = 5). (**C**) Effect of QRSJ on the gene expression of *Col1a* in lung tissues of PF mice induced by BLM (n = 3). (**D**) Effect of QRSJ on the gene expression of *Fn1* in lung tissues of PF mice induced by BLM (n = 3). (**E**) Immunofluorescence staining was performed, with imaging for lumican (pink), and staining with DAPI for nucleus (blue). Scale bar, 50 μm or 20 μm (Zoom). (**F**) Quantitative analysis of the mean fluorescence intensity of lumican (n = 3). The data is presented as mean ± SD, *$p < 0.01$, **$p < 0.01$ and ***$p < 0.001$ by one-way ANOVA. ns represents no significant difference.

group vs BLM group. It was found that pathways closely related to immune response and inflammatory response were widely enriched in TOP pathways (Figure 3D). These results indicated that QRSJ alleviates PF by affecting the immune microenvironment.

https://doi.org/10.2147/JIR.S479432

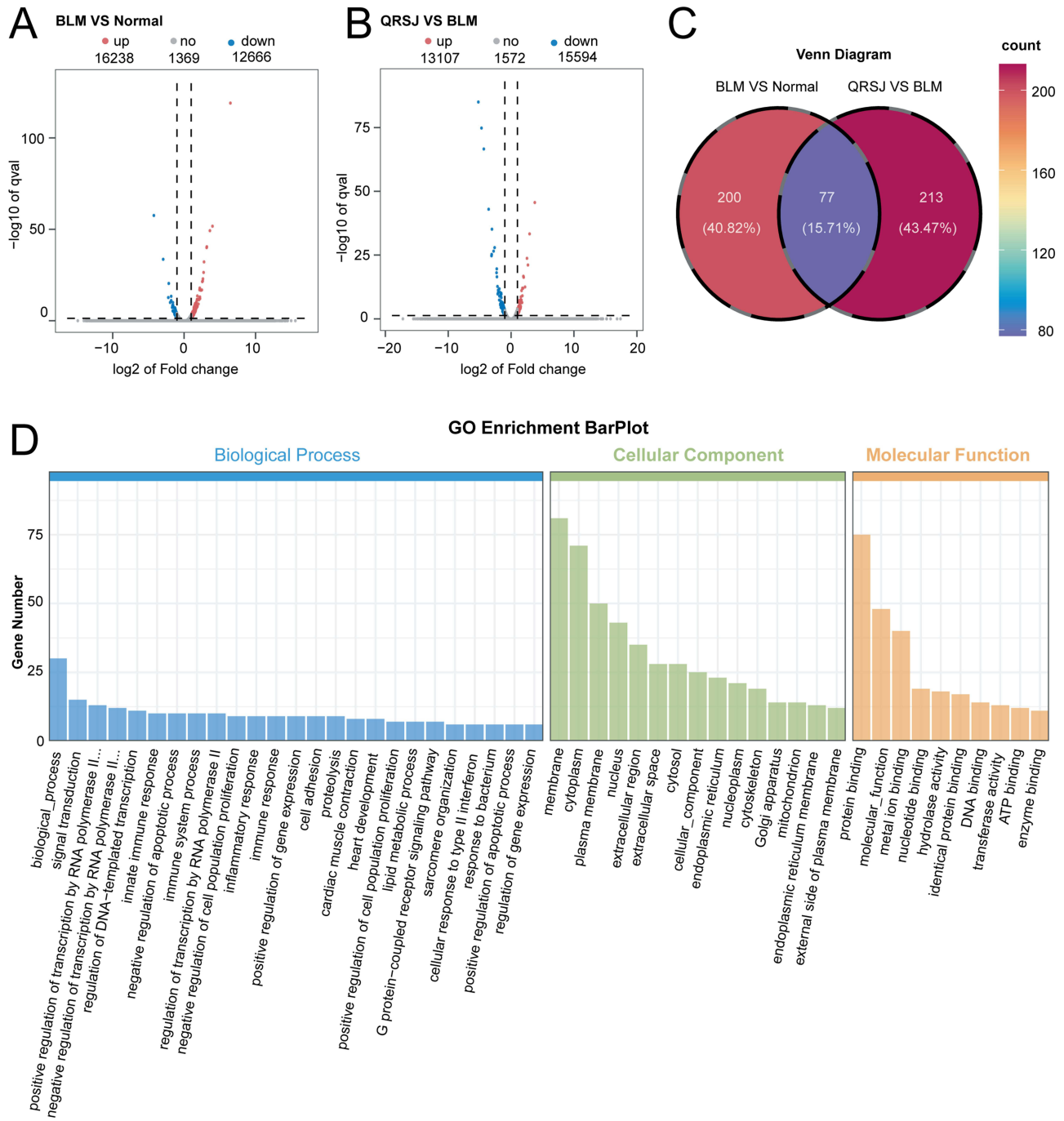

Figure 3 QRSJ alleviated PF through affecting immune microenvironment. (**A** and **B**) Volcano plot of differential mRNAs of group BLM group vs normal group or BLM+QRSJ group vs BLM group. (**C**) Venn diagram of differential genes of group BLM group vs normal group and BLM+QRSJ group vs BLM group. (**D**) GSEA enrichment pathway of differential mRNAs from BLM+QRSJ group vs BLM group.

QRSJ Improved Immune Cell Infiltration Induced by BLM

In fibrotic lung tissue, there is usually an infiltration of immune cells, particularly neutrophils.[17,34] To investigate whether QRSJ improves immune cell infiltration in lung tissue, we conducted immunofluorescence experiments to observe the expression of CD45 and Ly6G. Mice in the BLM group showed high levels of immune cell infiltration into lung tissues, indicating an inflammatory response to BLM. QRSJ administration significantly inhibited the expression of CD45 and attenuated BLM-induced immune cell infiltration in a dose-dependent manner (Figure 4A). Similar to these results, we

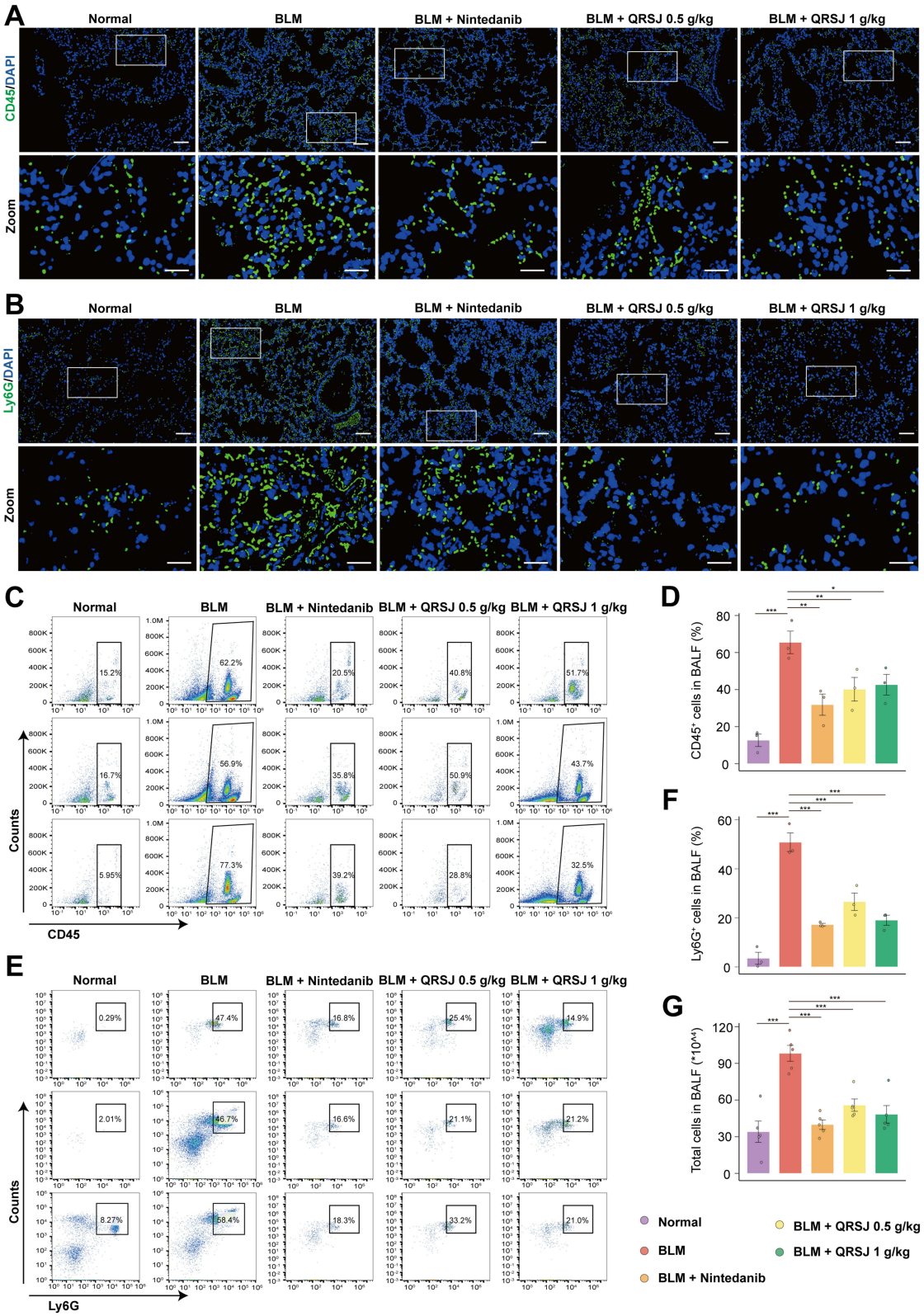

Figure 4 QRSJ improved immune cell infiltration induced by BLM. (**A**) Immunofluorescence staining was performed, with imaging for CD45 (green), and staining with DAPI for nucleus (blue). Scale bar, 50 μm or 20 μm (Zoom). (**B**) Immunofluorescence staining was performed, with imaging for Ly6G (green), and staining with DAPI for nucleus (blue). Scale bar, 50 μm or 20 μm (Zoom). (**C**) Detection of CD45 expression in BALF by flow cytometry. (**D**) The proportion of immune cells in BALF according to the data of flow cytometry (n = 3). (**E**) Detection of Ly6G expression in BALF by flow cytometry. (**F**) The proportion of neutrophils in BALF according to the data of flow cytometry (n = 3). (**G**) Statistical analysis of cells in BALF (n = 5). The data is presented as mean ± SD, *$p < 0.05$, **$p < 0.01$ and ***$p < 0.001$ by one-way ANOVA.

https://doi.org/10.2147/JIR.S479432

also found that compared with the normal group, BLM significantly increased the expression of Ly6G and induced neutrophil infiltration in lung tissues; whereas compared with the BLM group, the expression of Ly6G in the QRSJ+BLM group was reduced (Figure 4B). Besides, The number of immune cells in the BALF of the PF mice increased dramatically, while those of the 0.5 g/kg and 1 g/kg QRSJ group decreased (Figure 4C and D). The QRSJ down-regulated the number of neutrophils (Figure 4E and F). Moreover, the total cells in the BALF of the PF mice increased markedly, and it was reduced in the QRSJ group (Figure 4G). These data suggested that QRSJ improves immune cell infiltration induced by BLM.

QRSJ Alleviated the Release of Inflammatory Factors During the Progression of PF

NE is a major inflammatory protease released by neutrophils and is present in the airways of patients with cystic fibrosis, chronic obstructive pulmonary disease, non-cystic fibrosis bronchiectasis, and bronchopulmonary dysplasia.[35] Considering that QRSJ inhibited the infiltration of neutrophils in lung tissue, we next evaluated the effect of QRSJ on NE. Immunofluorescence experiments confirmed that QRSJ improved the distribution of NE in lung tissue during the progression of PF (Figure 5A and B). Similarly, QRSJ down-regulated the level of NE in serum of mice (Figure 5C). These results further confirmed the potential impact of QRSJ on neutrophils. To explore the impacts of QRSJ on inflammatory cytokines, we detected typical cytokines in the BALF and serum of mice, such as IL-1β, IL-6, TNF-α, and CXCL15. The BLM group showed significantly high levels of inflammatory cytokines. However, administration of QRSJ effectively reduced the levels of cytokines contrasted with the BLM group (Figure 5D–I). These results indicated that QRSJ alleviated the release of inflammatory factors during the progression of PF.

Effect of QRSJ on HMGB1 Expression

As a danger signal molecule, HMGB1 has the function of proinflammation and is closely involved in diverse fibrotic diseases, including renal fibrosis, liver fibrosis, and PF. Besides, different intervention approaches to inhibit HMGB1 release or its related signaling can reverse the experimental models of fibrotic diseases. Here, we found that the expression of HMGB1 in BLM group was markedly increased when compare to normal group (Figure 6A and B). Whereas QRSJ could significantly reduce the expression levels of HMGB1 in BALF, serum, and lung tissues when compare to BLM group (Figure 6C–E). It suggests that the protective effect of QRSJ may be due to the regulation of HMGB1 release and its pro-fibrotic process.

Discussion

PF occurs in a variety of clinical settings, constitutes a major cause of morbidity and mortality, and represents an enormous unmet medical need. It is characterized by abnormal multi-source proliferation of fibroblasts, as well as the overproduction, deposition, and disorganized degradation of collagen and other ECM. It remains a refractory and complex lung disease that can eventually lead to fatal lung failure, has a poor prognosis, and still lacks effective treatment strategies. Pirfenidone and nintedanib are approved for the treatment of PF based on their ability to slow functional decline and disease progression.[36–38] However, they do not offer a cure and are associated with tolerability issues.

Traditional Chinese medicines are generally used clinically to treat various diseases and have a significant effect. In this study, BLM was injected into the trachea to replicate the mouse model of PF, and the potential effects and potential mechanism of QRSJ on PF were elucidated. QRSJ was then demonstrated to alleviate the pathological changes and inhibit abnormal collagen production. These results confirm that QRSJ may be a therapeutic drug for PF. However, due to the complexity of the components in traditional Chinese medicine formulas, the anti-PF effects of QRSJ are very likely the result of synergistic actions through multiple targets and pathways.

Many studies have reported that cytokine and growth factor signaling pathways play important roles in fibroblast accumulation, differentiation and collagen production. Fibroblast and immune cell crosstalk has emerged as a critical process in promoting an efficient wound healing response.[39] Wound healing is regulated via overlapping immune responses associated with migration and proliferation of various cell types, the deposition of ECM and tissue remodeling.[40,41] In this study, we found that QRSJ significantly affected the immune microenvironment of lung tissue, particularly by inhibiting neutrophil infiltration. Furthermore, QRSJ inhibited the expression of IL-1β, IL-6, CXCL15 and TNF-α in the BALF and serum of mice.

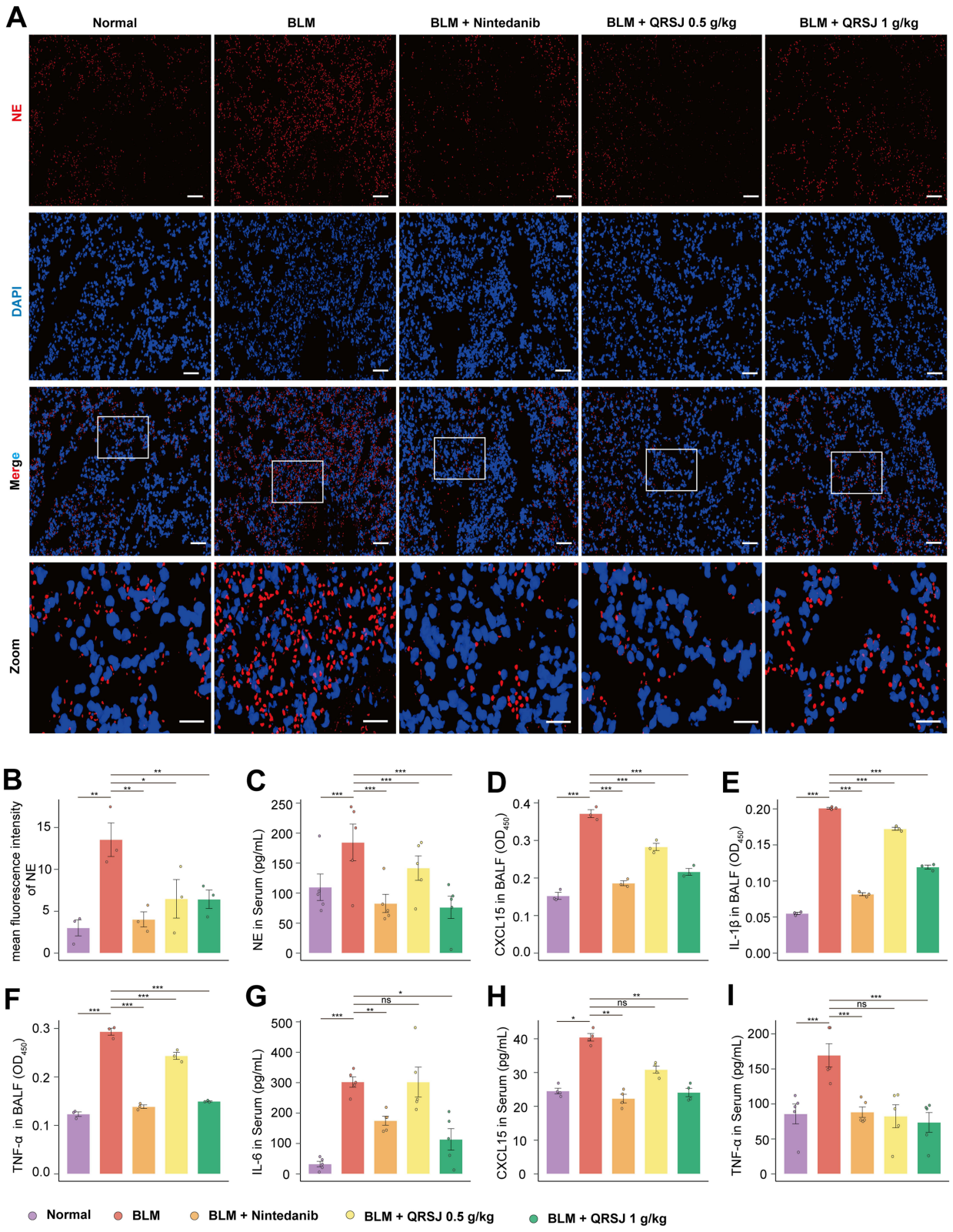

Figure 5 QRSJ alleviated the release of inflammatory factors during the progression of PF. (**A**) Immunofluorescence staining was performed, with imaging for NE (red), and staining with DAPI for nucleus (blue). Scale bar, 50 μm or 20 μm (Zoom). (**B**) Quantitative analysis of the mean fluorescence intensity of NE (n = 3). (**C**) The effect of QRSJ on the levels of NE in serum in different groups using ELISA (n = 5). (**D-F**) The effect of QRSJ on the levels of CXCL15, IL-1β and TNF-α in BALF in different groups using ELISA (n = 3). (**G**) The effect of QRSJ on the levels of IL-6 in serum in different groups using ELISA (n = 5). (**H**) The effect of QRSJ on the levels of CXCL15 in serum in different groups using ELISA (n = 4). (**I**) The effect of QRSJ on the levels of TNF-α in serum in different groups using ELISA (n = 5). The data is presented as mean ± SD, *p < 0.05, **p < 0.01 and ***p < 0.001 by one-way ANOVA. ns represents no significant difference.

https://doi.org/10.2147/JIR.S479432

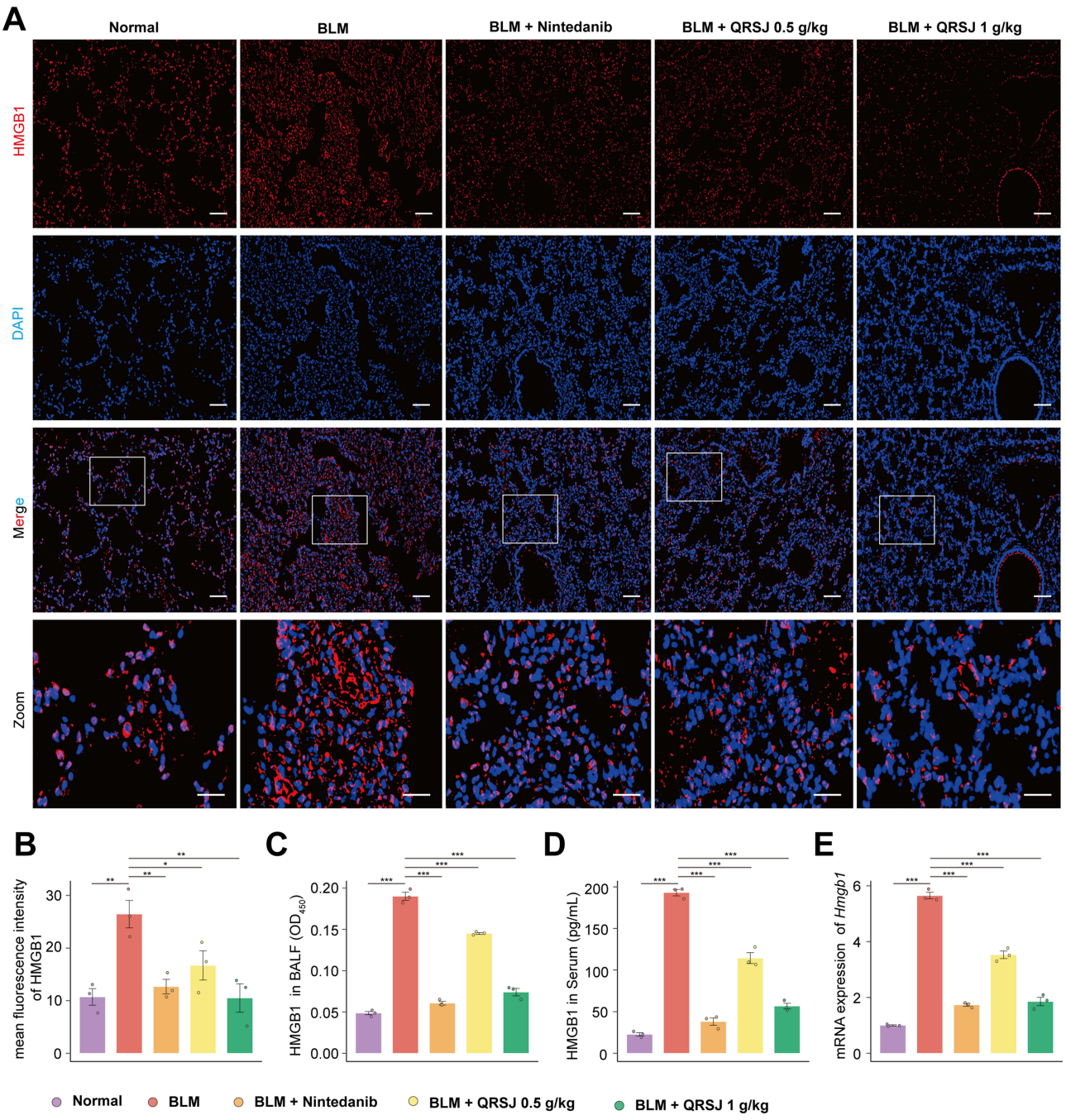

Figure 6 Effects of QRSJ on HMGB1 expression in mice with PF. (**A**) Immunofluorescence staining was performed, with imaging for HMGB1 (red), and staining with DAPI for nucleus (blue). Scale bar, 50 μm or 20 μm (Zoom). (**B**) Quantitative analysis of the mean fluorescence intensity of HMGB1. (**C**) The level of HMGB1 in BALF determined by ELISA. (**D**) The level of HMGB1 in serum determined by ELISA. (**E**) Effect of QRSJ on the gene expression of *Hmgb1* in lung tissues of PF mice induced by BLM. The data is presented as mean ± SD (n = 3), $*p < 0.05$, $**p < 0.01$ and $***p < 0.001$ by one-way ANOVA.

These results indicate that QRSJ primarily improves PF by affecting the immune microenvironment in the lung tissue. Many studies show that neutrophils play an important role in the continuous progression of both acute and chronic respiratory diseases.[42–45] Particularly, NE is a major inflammatory protease released by neutrophils and is present in the airways of patients with cystic fibrosis, chronic obstructive pulmonary disease, non- cystic fibrosis bronchiectasis, and bronchopulmonary dysplasia.[35] Interestingly, we found that QRSJ significantly reduced the proportion of neutrophils in lung tissue, as well as the content of NE. This suggests to some extent that QRSJ may primarily exert its role in regulating the immune microenvironment by affecting the function of neutrophils.

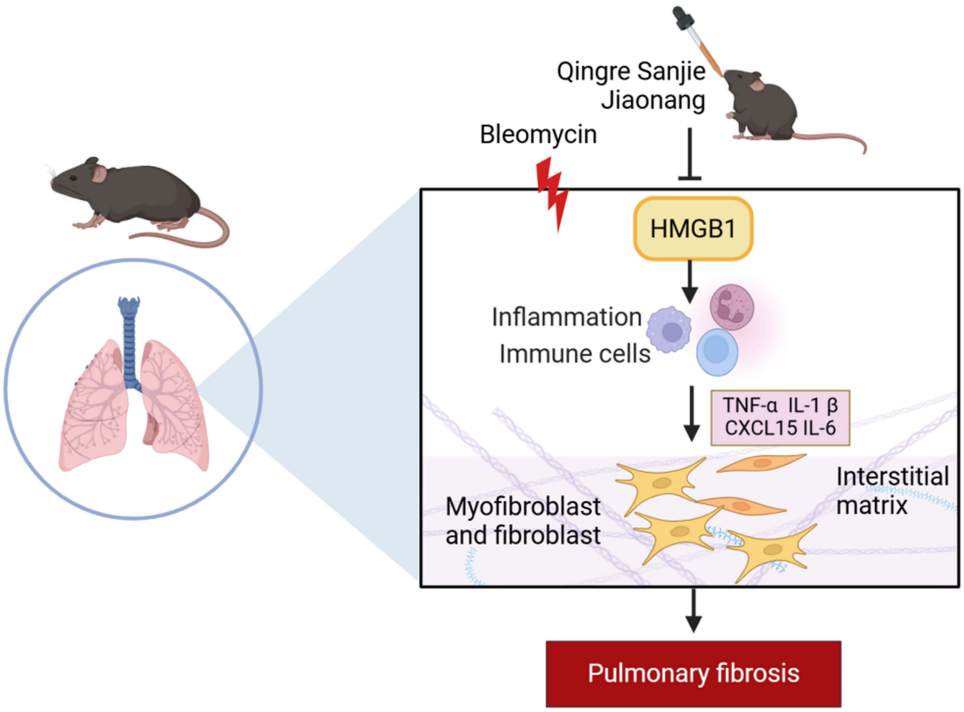

Figure 7 QRSJ improved PF through regulating HMGB1 release. Created in BioRender. Li, L. (2025) https://BioRender.com/t49tuf0.

To our knowledge, HMGB1, an injury-related model molecule, is essential for predicting disease progression in many diseases.[46–48] HMGB1 also plays an important role in the occurrence and development of PF.[20] Thus, inhibition of HMGB1 should represent a possible intervention strategy for PF. QRSJ has been clinically used for upper respiratory tract inflammation, acute bronchitis and other diseases.[10] There is no evidence to clarify whether QRSJ has a protective effect on PF and whether it plays a role in regulating the release of HMGB1, a mediator of lung injury and PF. In this study, QRSJ was then demonstrated to reduce the release of HMGB1 in the BALF, serum and lung tissues in mice with PF. We confirmed for the first time that QRSJ has ameliorative effects on PF, and its mechanism may be related to inhibiting collagen secretion and regulating excessive release of inflammatory factor HMGB1 (Figure 7). This study provides certain theoretical value and clinical significance to elucidate the lung protection role of QRSJ and gives full play to the advantages of traditional Chinese medicine in treating PF.

However, there are many other interesting points to address. First of all, this pilot study only explored that QRSJ may improve PF by regulating the release of HMGB1, and whether other mediators and downstream signals of HMGB1 are involved in the regulatory mechanism is unclear. Further in vitro researches focusing on the mechanism and drug efficacy are needed. Secondly, in order to further verify its role, it is intended to collect cases of PF in the clinic and adopt the treatment scheme of combined QRSJ to explore its improvement effects on the symptoms and indicators of PF. Thirdly, as glucocorticoids are still the main drugs in the clinical treatment of PF, whether QRSJ combined with glucocorticoids is better than the effects of glucocorticoids in the treatment of PF is still unclear. Fourthly, HMGB1 may be used as a therapeutic protein for PF, and the future exploration and development of new monoclonal antibodies or inhibitors of HMGB1 may provide novel ideas for the diagnosis and treatment of the fibrotic diseases.

Conclusion

In summary, this study demonstrated the benefits of QRSJ in improving the pathological abnormalities in a PF model, revealing the new potential of the old drug. It should be attributed to the regulation of abnormal immune microenvironment and HMGB1 release. Future efforts should focus on its specific pharmacological mechanisms and clinical outcomes.

Acknowledgment

We gratefully acknowledge Wencheng Zhou (The First Affiliated Hospital of Zhejiang Chinese Medical University) and Zhisen Wang (Zhejiang Hospital) for methodological guidance in optimizing the research design, implementing and completing the supplementary experiments, and providing technical assistance in data interpretation, and Jingduo Li (Shanghai General Hospital) for reviewing the revised manuscript for scientific accuracy during the revision. Their intellectual contributions significantly enhanced the scientific rigor of this study.

Author Contributions

All authors made a significant contribution to the work reported, whether in the conception, review design, execution, acquisition of data, analysis, and interpretation, or in all these areas, took part in drafting, revising, or critically reviewing the article; gave final approval of the version to be published; have agreed on the journal to which the article has been submitted; and agree to be accountable for all aspects of the work.

Funding

This study was supported by the Zhejiang Provincial Science Technology Projects of Traditional Chinese Medicine (Nos. 2021ZB174 and 2021ZB301) and Zhejiang Provincial Natural Science Foundation of China (No. LYY19H280006).

Disclosure

All authors declare no conflicts of interest in this work.

References

1. Moss BJ, Ryter SW, Rosas IO. Pathogenic mechanisms underlying idiopathic pulmonary fibrosis. *Annu Rev Pathol*. 2022;17:515–546. doi:10.1146/annurev-pathol-042320-030240
2. Oldham JM, Vancheri C. Rethinking idiopathic pulmonary fibrosis. *Clin Chest Med*. 2021;42(2):263–273. doi:10.1016/j.ccm.2021.03.005
3. Thannickal VJ, Toews GB, White ES, et al. Mechanisms of pulmonary fibrosis. *Annu Rev Med*. 2004;55(1):395–417. doi:10.1146/annurev.med.55.091902.103810
4. Man RK, Gogikar A, Nanda A, et al. A comparison of the effectiveness of nintedanib and pirfenidone in treating idiopathic pulmonary fibrosis: a systematic review. *Cureus*. 2024;16(2):e54268. doi:10.7759/cureus.54268
5. Chianese M, Screm G, Salton F, et al. Pirfenidone and nintedanib in pulmonary fibrosis: lights and shadows. *Pharmaceuticals*. 2024;17(6):709. doi:10.3390/ph17060709
6. Li Z, Feiyue Z, Gaofeng L. Traditional Chinese medicine and lung cancer--From theory to practice. *Biomed Pharmacother*. 2021;137:111381. doi:10.1016/j.biopha.2021.111381
7. Huang K, Zhang P, Zhang Z, et al. Traditional Chinese medicine (TCM) in the treatment of COVID-19 and other viral infections: efficacies and mechanisms. *Pharmacol Ther*. 2021;225:107843. doi:10.1016/j.pharmthera.2021.107843
8. Cao X, Wang Y, Chen Y, et al. Advances in traditional Chinese medicine for the treatment of chronic obstructive pulmonary disease. *J Ethnopharmacol*. 2023;307:116229. doi:10.1016/j.jep.2023.116229
9. Wang D, Huang L, Chen S. Senecio scandens Buch.-Ham.: a review on its ethnopharmacology, phytochemistry, pharmacology, and toxicity. *J Ethnopharmacol*. 2013;149(1):1–23. doi:10.1016/j.jep.2013.05.048
10. Yu J, Hu M, Wang Y, et al. Extraction, partial characterization and bioactivity of polysaccharides from Senecio scandens Buch.-Ham. *Int J Biol Macromol*. 2018;109:535–543. doi:10.1016/j.ijbiomac.2017.12.119
11. Koudstaal T, Funke-Chambour M, Kreuter M, et al. Pulmonary fibrosis: from pathogenesis to clinical decision-making. *Trends Mol Med*. 2023;29(12):1076–1087. doi:10.1016/j.molmed.2023.08.010
12. Ghonim MA, Boyd DF, Flerlage T, et al. Pulmonary inflammation and fibroblast immunoregulation: from bench to bedside. *J Clin Invest*. 2023;133(17):e170499. doi:10.1172/JCI170499
13. Heukels P, Moor CC, von der Thusen JH, et al. Inflammation and immunity in IPF pathogenesis and treatment. *Respir Med*. 2019;147:79–91. doi:10.1016/j.rmed.2018.12.015
14. Liu G, Philp AM, Corte T, et al. Therapeutic targets in lung tissue remodelling and fibrosis. *Pharmacol Ther*. 2021;225:107839. doi:10.1016/j.pharmthera.2021.107839
15. Gieseck RL, Wilson MS, Wynn TA. Type 2 immunity in tissue repair and fibrosis. *Nat Rev Immunol*. 2018;18(1):62–76. doi:10.1038/nri.2017.90
16. Kumar V, hertz M, Agro A, et al. Type 1 invariant natural killer T cells in chronic inflammation and tissue fibrosis. *Front Immunol*. 2023;14:1260503. doi:10.3389/fimmu.2023.1260503
17. Kolahian S, Fernandez IE, Eickelberg O, et al. Immune mechanisms in pulmonary fibrosis. *Am J Respir Cell mol Biol*. 2016;55(3):309–322. doi:10.1165/rcmb.2016-0121TR
18. Andersson U, Ottestad W, Tracey KJ. Extracellular HMGB1: a therapeutic target in severe pulmonary inflammation including COVID-19? *Mol Med*. 2020;26(1):42. doi:10.1186/s10020-020-00172-4
19. Xue J, Suarez JS, Minaai M, et al. HMGB1 as a therapeutic target in disease. *J Cell Physiol*. 2021;236(5):3406–3419. doi:10.1002/jcp.30125
20. Li LC, Gao J, Li J. Emerging role of HMGB1 in fibrotic diseases. *J Cell Mol Med*. 2014;18(12):2331–2339. doi:10.1111/jcmm.12419
21. Chen R, Kang R, Tang D. The mechanism of HMGB1 secretion and release. *Exp Mol Med*. 2022;54(2):91–102. doi:10.1038/s12276-022-00736-w

22. Tang D, Kang R, Zeh HJ, et al. The multifunctional protein HMGB1: 50 years of discovery. *Nat Rev Immunol*. 2023;23(12):824–841. doi:10.1038/s41577-023-00894-6
23. Li LC, Xu L, Hu Y, et al. Astragaloside IV improves bleomycin-induced pulmonary fibrosis in rats by attenuating extracellular matrix deposition. *Front Pharmacol*. 2017;8:513. doi:10.3389/fphar.2017.00513
24. Li LC, Li DL, Xu L, et al. High-mobility group box 1 mediates epithelial-to-mesenchymal transition in pulmonary fibrosis involving transforming growth factor-beta1/Smad2/3 signaling. *J Pharmacol Exp Ther*. 2015;354(3):302–309. doi:10.1124/jpet.114.222372
25. Cui W, Li L, Li D, et al. Total glycosides of Yupingfeng protects against bleomycin-induced pulmonary fibrosis in rats associated with reduced high mobility group box 1 activation and epithelial-mesenchymal transition. *Inflamm Res*. 2015;64(12):953–961. doi:10.1007/s00011-015-0878-x
26. Li L, Li D, Xu L, et al. Total extract of Yupingfeng attenuates bleomycin-induced pulmonary fibrosis in rats. *Phytomedicine*. 2015;22(1):111–119. doi:10.1016/j.phymed.2014.10.011
27. Li Y, Yuan Y, Huang ZX, et al. GSDME-mediated pyroptosis promotes inflammation and fibrosis in obstructive nephropathy. *Cell Death Differ*. 2021;28(8):2333–2350. doi:10.1038/s41418-021-00755-6
28. She S, Wu X, Zheng D, et al. PSMP/MSMP promotes hepatic fibrosis through CCR2 and represents a novel therapeutic target. *J Hepatol*. 2020;72(3):506–518. doi:10.1016/j.jhep.2019.09.033
29. Liu Y, Chen L, Gao L, et al. LRRK2 deficiency protects the heart against myocardial infarction injury in mice via the P53/HMGB1 pathway. *Free Radic Biol Med*. 2022;191:119–127. doi:10.1016/j.freeradbiomed.2022.08.035
30. Hubner RH, Gitter W, El Mokhtari NE, et al. Standardized quantification of pulmonary fibrosis in histological samples. *Biotechniques*. 2008;44(4):507–511, 514–507. doi:10.2144/000112729
31. Snijder J, Peraza J, Padilla M, et al. Pulmonary fibrosis: a disease of alveolar collapse and collagen deposition. *Expert Rev Respir Med*. 2019;13(7):615–619. doi:10.1080/17476348.2019.1623028
32. Wynn TA. Cellular and molecular mechanisms of fibrosis. *J Pathol*. 2008;214(2):199–210. doi:10.1002/path.2277
33. Wang Z, Gerstein M, Snyder M. RNA-Seq: a revolutionary tool for transcriptomics. *Nat Rev Genet*. 2009;10(1):57–63. doi:10.1038/nrg2484
34. Xu Y, Lan P, Wang T. The role of immune cells in the pathogenesis of idiopathic pulmonary fibrosis. *Medicina*. 2023;59(11):1984. doi:10.3390/medicina59111984
35. Voynow JA, Shinbashi M. Neutrophil elastase and chronic lung disease. *Biomolecules*. 2021;11(8):1065. doi:10.3390/biom11081065
36. Moua T, Baqir M, Ryu JH. What is on the horizon for treatments in idiopathic pulmonary fibrosis? *J Clin Med*. 2024;13(21):6304.
37. Spagnolo P, Kropski JA, Jones MG, et al. Idiopathic pulmonary fibrosis: disease mechanisms and drug development. *Pharmacol Ther*. 2021;222:107798. doi:10.1016/j.pharmthera.2020.107798
38. Karampitsakos T, Tourki B, Herazo-Maya JD. The Dawn of precision medicine in fibrotic interstitial lung disease. *Chest*. 2024. doi:10.1016/j.chest.2024.10.042
39. Ishida Y, Kuninaka Y, Mukaida N, et al. Immune mechanisms of pulmonary fibrosis with bleomycin. *Int J mol Sci*. 2023;24(4):3149. doi:10.3390/ijms24043149
40. Mutsaers SE, Miles T, Prele CM, et al. Emerging role of immune cells as drivers of pulmonary fibrosis. *Pharmacol Ther*. 2023;252:108562. doi:10.1016/j.pharmthera.2023.108562
41. Zhang WJ, Chen SJ, Zhou SC, et al. Inflammasomes and fibrosis. *Front Immunol*. 2021;12:643149. doi:10.3389/fimmu.2021.643149
42. Cui X, Li T, Yang J, et al. Predictive value of dsDNA and nucleosomes as neutrophil extracellular traps-related biomarkers for COVID-19 in older patients. *J Inflamm Res*. 2024;17:8831–8838. doi:10.2147/JIR.S414688
43. Wang ZZ, Li H, Maskey AR, et al. The efficacy & molecular mechanisms of a terpenoid compound ganoderic acid C1 on corticosteroid-resistant neutrophilic airway inflammation: in vivo and in vitro validation. *J Inflamm Res*. 2024;17:2547–2561. doi:10.2147/JIR.S433430
44. Zhang XH, Han MF, Teng XB, et al. Combined inflammatory markers for predicting acute exacerbations in chronic obstructive pulmonary disease with respiratory failure. *J Inflamm Res*. 2025;18:2513–2520. doi:10.2147/JIR.S508048
45. Zou S, Jie H, Han X, et al. The role of neutrophil extracellular traps in sepsis and sepsis-related acute lung injury. *Int Immunopharmacol*. 2023;124(Pt A):110436. doi:10.1016/j.intimp.2023.110436
46. Qu X, Hou X, Zhu K, et al. Neutrophil extracellular traps facilitate sympathetic hyperactivity by polarizing microglia toward M1 phenotype after traumatic brain injury. *FASEB J*. 2023;37(9):e23112. doi:10.1096/fj.202300752R
47. Yang X, Pan Y, Cai L, et al. Calycosin ameliorates neuroinflammation via TLR4-mediated signal following cerebral ischemia/reperfusion injury in vivo and in vitro. *J Inflamm Res*. 2024;17:10711–10727. doi:10.2147/JIR.S480262
48. Cheng Z, Li X, Wang S, et al. High translocation of high mobility group box 1 in the brain tissue of patients with Sturge-Weber syndrome. *J Inflamm Res*. 2024;17:9347–9358. doi:10.2147/JIR.S473377